

This is a repository copy of Optimal Fast-Acting Frequency Containment for Modern Power Systems with Variable Inertia.

White Rose Research Online URL for this paper: <a href="https://eprints.whiterose.ac.uk/id/eprint/233280/">https://eprints.whiterose.ac.uk/id/eprint/233280/</a>

Version: Accepted Version

# **Proceedings Paper:**

Azizi, S. (Accepted: 2025) Optimal Fast-Acting Frequency Containment for Modern Power Systems with Variable Inertia. In: Proceedings of 2025 IEEE International Conference on Energy Technologies for Future Grids. 2025 IEEE International Conference on Energy Technologies for Future Grids, 07-11 Dec 2025, Wollongong, Australia. IEEE. (In Press)

This is an author produced version of a conference paper accepted for publication in Proceedings of 2025 IEEE International Conference on Energy Technologies for Future Grids, made available under the terms of the Creative Commons Attribution License (CC-BY), which permits unrestricted use, distribution and reproduction in any medium, provided the original work is properly cited.

# Reuse

This article is distributed under the terms of the Creative Commons Attribution (CC BY) licence. This licence allows you to distribute, remix, tweak, and build upon the work, even commercially, as long as you credit the authors for the original work. More information and the full terms of the licence here: https://creativecommons.org/licenses/

#### Takedown

If you consider content in White Rose Research Online to be in breach of UK law, please notify us by emailing eprints@whiterose.ac.uk including the URL of the record and the reason for the withdrawal request.



# Optimal Fast-Acting Frequency Containment for Modern Power Systems with Variable Inertia

Sadegh Azizi University of Leeds s.azizi@leeds.ac.uk

Abstract—This paper proposes an Optimal Fast Frequency Containment (OFFC) approach during loss-of-generation (LoG) events, combining analytical derivation with an optimization framework for resource deployment. The system frequency response is modeled by a second-order power-frequency transfer function, enabling a closed-form characterization of the optimal power injection profile. This profile maximizes the frequency nadir for a given energy input. Building on this, a scalable optimization framework is established to realize the target injection using available generation resources, each represented by a trapezoidal power profile. A novel linear formulation is developed to model the trapezoidal ramping without bilinear terms. This ensures scalability and guarantees global optimality under operational constraints such as ramp limits, delays, and energy capacities. The proposed approach supports real-time deployment decisions while accounting for resource diversity, facilitating greater integration of renewable energy sources.

Keywords—Laplace transform, optimal fast-acting frequency containment (OFFC), optimization, system frequency response (SFR).

## I. INTRODUCTION

Fast-acting frequency containment (FFC) refers to the deliberate, rapid injection of active power into a power system to arrest frequency decline during the first critical seconds following a loss-of-generation (LoG) event, before the nadir is reached [1]. FFC has become a key mechanism for maintaining frequency stability in systems with high penetration of renewable energy sources (RESs), where synchronous inertia is low and variable [2], [3]. Contrary to 'fast frequency response,' a term that can also denote the natural post-disturbance frequency behavior of the system, FFC is the preferred terminology as it exclusively refers to a controlled intervention to mitigate frequency deviations.

The importance of FFC has grown with the increasing variability of system inertia, driven by the displacement of synchronous generation by RESs [4, 5]. Inertia levels now fluctuate not only seasonally and diurnally but also in response to short-term weather patterns affecting wind and solar output. When system inertia is highly reduced, the rate of change of frequency following an LoG event is higher, the nadir is lower, and the available response time is shorter [6, 7]. The 2019 UK and 2025 Iberian blackouts demonstrate the vulnerability of modern power systems under such conditions, where a combination of reduced inertia and limited fast reserves can easily contribute to widespread disruptions.

In operational practice, FFC can be delivered through a diverse portfolio of resources, each with distinct performance characteristics [3]. Synchronous machines contribute fast but

transient inertial energy, turbine governors provide a sustained adjustment over several seconds. Wind turbines can temporarily increase output by extracting kinetic energy from rotor inertia, and power electronics—based resources such as batteries and solar PV can deliver near-instantaneous injections with high precision [8]. Effective deployment requires coordination of these heterogeneous resources across multiple time layers [8]:

- Fast frequency containment (0.1–2 s): Batteries, synthetic inertia, and fast converter-based responses arrest the initial frequency decline.
- Primary control (2–30 s): Turbine-governor systems provide sustained frequency support.
- Secondary and tertiary control (>30 s): Slower adjustments restore frequency to nominal levels.

The work presented in this paper focuses on *Optimal Fast-acting Frequency Containment (OFFC)*—a targeted, short-duration injection strategy designed to reduce or eliminate the transient frequency deviation while preserving or improving the final steady-state value. This concept builds on the decomposition of frequency response into transient and steady-state components [1], and on the use of the inverse system frequency response (SFR) model to determine the exact magnitude, timing, and profile of corrective injections. The objective is to maximize the frequency nadir for a given available energy, thereby reducing the duration of low-frequency operations and avoiding unnecessary wear on mechanical resources.

This research work makes two key contributions. First, it provides an analytical derivation of optimal injection profiles by modelling the frequency deviation. Closed-form expressions are derived for the corrective power injection required to flatten the frequency trajectory over a specified time window. This helps maximize the frequency nadir for a fixed available energy. Second, it introduces a scalable deployment optimization framework for diverse generation resources. This is achieved through a linear, deterministic, and computationally efficient formulation for implementing OFFC. The optimization framework makes best use of available resources with different ramp rates, delays, and energy capacities. A novel technique is also set forth to represent trapezoidal injection profiles without introducing nonlinearities into the optimization framework.

The remainder of the paper is organized as follows. Section II derives closed-form expressions for optimal injection based on the inverse SFR approach. Section III presents the resource deployment framework, including the linearized trapezoidal representation and optimization constraints. Section IV

discusses implementation considerations and illustrates the approach through numerical studies. Section V concludes the paper.

#### II. OPTIMAL POWER INJECTION

The power system is modeled as a linear, time-invariant system when examining the relationship between power and frequency. This simplification makes it easier to express the differential equations that govern frequency dynamics. The average response of the center-of-inertia (CoI) frequency to changes in generation or load can be effectively captured using a second-order model, which balances the need to represent the key dynamic behavior with analytical simplicity [9]–[11].

The size of the LoG event is assumed to be detectable by the control center within sub-seconds of its occurrence [5]. Let  $\Delta F(s)$ ,  $\Delta P(s)$  and  $G_{SFR}(s)$  denote the frequency deviation, power disturbance, and SFR transfer function in the Laplace domain, respectively. With these, the frequency deviation following the power disturbance can be written as

$$\Delta F(s) = \Delta P(s) \times G_{SFR}(s) \tag{1}$$

where  $G_{SFR}(s)$  is a second-order minimum-phase transfer function in its simplified form approximated as [3, 30]:

$$G_{SFR}(s) = \overbrace{\left(\frac{R\omega_n^2}{DR + K_m}\right)} \left(\frac{1 + T_R s}{s^2 + 2\zeta\omega_n s + \omega_n^2}\right) \tag{2}$$

In this formula, the parameters R, D,  $K_m$ ,  $T_R$ ,  $\zeta$ , and  $\omega_n$  respectively represent the effects of the governor droop, frequency dependence of load, mechanical gain factor, reheat time constant, damping factor, and natural frequency of the system [30].

Let us assume the power disturbance in the per unit form is a step function with magnitude *P* as below

$$\Delta p(t) = Pu(t) \tag{3}$$

Given the SFR transfer function (2), the frequency deviation following this disturbance in the time domain is [9]:

$$\Delta f(t) = \Delta f_{ss} [1 - \csc \varphi \sin(\omega_d t + \varphi) e^{-\zeta \omega_n t}] u(t)$$
 (4)

where  $\Delta f_{ss} = P\gamma\omega_n^{-2}$ ,  $\csc\varphi$  represents the reciprocal of  $\sin\varphi$ , and  $\omega_d$  and  $\varphi$  are constants determined based on the SFR model parameters as detailed in [10]. The frequency response following an LoG event, opposite to (3), is equal to the pre-disturbance system frequency nominal frequency  $f_0$  minus (4), as shown below:

$$f(t) = [f_0 - \Delta f(t)]u(t) \tag{5}$$

It can be confirmed that  $\Delta f(t)$  also represents the response required to eliminate the frequency deviation caused by the LoG event. By defining  $\theta = \text{acos } \zeta$  (as shown in Fig. 1) and applying the inverse Laplace transform to (4),  $\Delta F(s)$  is obtained in terms of the parameters already defined as

$$\Delta F(s) = \frac{\Delta f_{ss}}{s} + K \left[ \frac{\sin \varphi \, s + \omega_n \sin(\varphi + \theta)}{(s + \zeta \omega_n)^2 + \omega_d^2} \right] \tag{6}$$

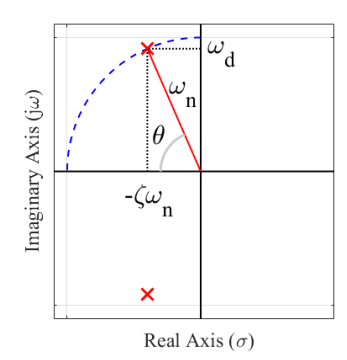


Fig. 1. Representation of pole positions for the SFR transfer function in the complex plane.

where  $\zeta \omega_n \sin \varphi + \omega_d \cos \varphi$  is replaced with  $\sin(\varphi + \theta)$  and K is defined as  $K = -\Delta f_{ss} \csc \varphi$ .

As demonstrated in [1], a flattened frequency response yields the highest nadir for a given amount of energy injection. Let  $\delta f(t)$  denote the required adjustment needed to flatten the frequency response described by (5) between  $t = t_1$  and  $t = t_2$ . For clarity and reuse,  $\delta f(t)$  is expressed in terms of two subfunctions as

$$\delta f(t) = m_{t_1}(t) - m_{t_2}(t) \tag{7}$$

where  $m_{\tau}(t) = [\Delta f(t) - f_{\tau}] u(t - \tau)$  for any  $\tau$  and  $f_{\tau} = f(\tau)$ . It can be seen that  $m_{\tau}(t)$  is essentially  $\Delta f(t)$ , zeroed before  $t = \tau$  and offset by  $-f_{\tau}$  to ensure the function equals zero at that time. Accordingly, expression (7) represents the portion of  $\Delta f(t)$  that lies between  $t = t_1$  and  $t = t_2$ , with the boundary value  $\Delta f_{t_1} = \Delta f_{t_2}$  subtracted off to ensure the portion starts and ends at zero.

The Laplace transform of  $m_{\tau}(t)$  is denoted by  $M_{\tau}(s)$  and the power injection needed to bring about this frequency response is denoted by  $\pi_{\tau}(t)$ . All of these functions, both in the time and Laplace domains, along with the closed-form solution for  $\pi_{\tau}(t)$  are detailed in Appendix. Now, let  $\delta P(t)$  denote the power injection that flattens frequency response between  $t_1$  and  $t_2$ . Using the derivations put forward so far, one can write

$$\delta p(t) = \pi_{t_1}(t) - \pi_{t_2}(t) \tag{8}$$

The stepped power disturbance  $\Delta p(t)$  produces a bell-shaped frequency response. Injecting  $\delta P(t)$  between  $t_1$  and  $t_2$  exactly flattens this response, yielding the optimal nadir for the available injected energy.

# III. RESOURCE DEPLOYMENT

An optimization framework is required to deliver the OFFC response across multiple generation resources during an LoG event. In principle, the system should be capable of realizing any appropriate active power injection profile, represented using trapezoidal injections distributed among participating resources. The primary objective is to minimize the aggregate mismatch between the desired and actual power injections, subject to the operational constraints of each resource. Deployment should prioritize technical effectiveness of

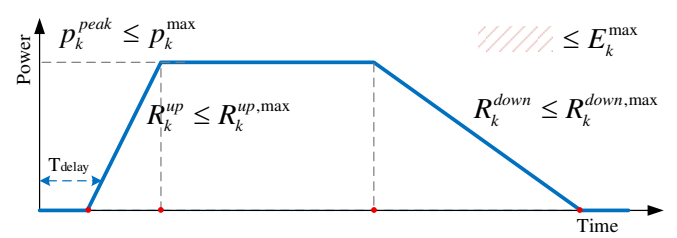


Fig. 2. Typical power characteristic of a generating resource providing FFC services.

frequency response rather than cost of provision [8]. The optimization explicitly accounts for heterogeneous response times, enabling efficient realization of the desired aggregate profile. The formulation presented in this section provides a tractable, deterministic, and scalable framework for real-time OFFC deployment, while respecting technical limits and resource diversity.

#### A. Operational Context

The dynamic frequency containment capability of a generation resource can be defined by a set of operational parameters that capture its behavior during an LoG event. This response is represented by a trapezoidal active power injection profile (Fig. 2), which describes the resource's output throughout the event. The profile begins after a time delay, defined as the latency between the system trigger (or dispatch instruction) and the start of power injection.

Following activation, the resource ramps up at a bounded ramp-up rate until reaching the required power level, up to its maximum capability. The sustained period at this level is constrained by the available energy, often determined by the state-of-charge. The withdrawal phase is governed by a bounded ramp-down rate to ensure a smooth reduction in output and avoid secondary system instabilities.

The exact ramp-up/down rates and start/finish times for each resource are not known a priori. Since delivered energy is the product of power and duration, uncertainty in both parameters introduces potential nonlinearities. To preserve analytical tractability, the trapezoidal injection is reformulated here using auxiliary variables and constraints, avoiding direct multiplication of decision variables. This approach is necessary to ensure computational efficiency, deterministic convergence, and global optimality within predefined tolerances, which are essential for real-time applications.

## B. Optimization Formulation

Performing optimization for resource deployment on a discretized spectrum is much easier than on a continuous one. Therefore, we discretize the period of interest into 100 intervals (without loss of generality), with the i —th time instant referring to  $t=(i-1)\Delta t$  (for i=1,...,100). Let us assume  $\delta p_i^{trgt}$  refers to the target power we aim to deliver at i—th time slot. This can be obtained based on (8) or its simplified triangular approximations introduced in [1]. Let  $p_i^{inj}$  signify the collective response of resources (in terms of active power injection) across the system at the i—th instant. Ideally, we would prefer that  $\delta p_i^{trgt} = p_i^{inj}$  for  $\forall i$ . However, this assumption may be overly

optimistic given the operational constraints of the available resources. Consequently, the optimization must seek to minimize the cumulative least absolute deviation between the actual and target injections over the discretized time horizon.

To establish the optimization formulation, first, let us assume we have m providers that can be instructed to participate in frequency containment upon need. In this context, let  $p_g(k,i)$  refer to the injection of the k-th resource at the i-th time instant. Therefore,

$$p_i^{inj} = \sum_{k=1}^m p_g(k, i) \tag{9}$$

Now, an optimization framework is needed to achieve the following objective

$$\min \sum_{i=1}^{N} \left| \delta p_i^{trgt} - p_i^{inj} \right| \tag{10}$$

A key innovation of this work is the linear representation of trapezoidal injections without multiplying decision variables, using a neighbor-average property: in a trapezoid, the average of two non-neighboring points on opposite slopes cannot equal either edge value. In the discretized domain, each trapezoid spans at least four instants—three in the limiting triangular case where maximum output occurs at only one instant. Thus, if two non-neighboring points are separated by two instants, they must lie on opposite slopes. Exploiting this property preserves linearity, enabling tractable optimization.

We define four sets of binary auxiliary variables a(k,i), b(k,i), c(k,i), d(k,i) to represent the positions of the four edges of a trapezoidal power profile for unit k. For the first set, the constraint

$$\sum_{i=1}^{N} a(k,i) = 1, \quad \forall k$$
 (11)

and analogously for the three other sets ensures that exactly one position is selected, thereby uniquely identifying each trapezoid edge in time. To facilitate sequencing, we introduce cumulative binary variables. A(k,i), B(k,i), C(k,i), D(k,i), defined such that

$$\sum_{j=1}^{i} a(k,j) \le A(k,i), \quad \forall k,i$$
 (12)

with analogous definitions for B(k,i), C(k,i), D(k,i). The ordering constraints

$$A(k,i) < B(k,i) \le C(k,i) < D(k,i) \qquad \forall k,i \tag{13}$$

along with (12) guarantee that the first and only "1" in each of the arrays a(k,.), b(k,.), c(k,.) and d(k,.) appears in the correct chronological order. This is to preserve the intended sequencing of trapezoid edge positions.

Let  $R_k^{up,max}$  and  $R_k^{down,max}$  denote the maximum ramp-up and ramp-down rates of unit k, respectively. Variables  $H^a(k,i)$ ,  $H^b(k,i)$ ,  $H^c(k,i)$  and  $H^d(k,i)$  are introduced to represent the incremental change between each trapezoidal edge and its neighboring points, corresponding to the first, second, third, and

fourth edges, respectively. For  $\forall k$  and i, these variables are constrained as

$$\begin{cases} 0 \leq H^{a}(k,i) \leq \frac{a(k,i)R_{k}^{up,max}}{2} \\ -\frac{b(k,i)R_{k}^{up,max}}{2} \leq H^{b}(k,i) \leq 0 \\ -\frac{c(k,i)R_{k}^{down,max}}{2} \leq H^{c}(k,i) \leq 0 \\ 0 \leq H^{d}(k,i) \leq \frac{d(k,i)R_{k}^{down,max}}{2} \end{cases}$$

$$(14)$$

to ensure that slope changes occur only at the designated edges and remain within the specified ramp limits. To enforce zero slope when the unit reaches its peak power, the following equality constraints are imposed:

$$\begin{cases} \sum_{i=1}^{i=N} H^{a}(k,i) = -\sum_{i=1}^{i=N} H^{b}(k,i), & \forall k \\ \sum_{i=1}^{i=N} H^{c}(k,i) = -\sum_{i=1}^{i=N} H^{d}(k,i), & \forall k \end{cases}$$
(15)

The absolute value of the two sides of the first equality represents half of the unit's ramp-up rate  $R_k^{up}$ , while the second equality similarly represents half of the ramp-down rate  $R_k^{down}$ . The resulting trapezoidal profile has a maximum of three segments with zero slope, one ramp-up segment at  $R_k^{up}$  and one ramp-down segment at  $R_k^{down}$ . The auxiliary variable s(k,i) is used here to mark not only the four edge points where slope changes occur for unit k but also quantify the magnitude of these changes. In this context, s(k,i) is defined as

$$s(k,i) = 2[H^a(k,i) + H^b(k,i) + H^c(k,i) + H^d(k,i)]$$
 (16)

Now, one can easily use this variable to recursively calculate the unit's power output for  $\forall k$  from

$$p_a(k,i) = 2p_a(k,i-1) - p_a(k,i-2) + s(k,i-1)$$
(17)

For the initial time steps, the fictitious values  $p_g(k,-1)$ ,  $p_g(k,0)$  and s(k,0) are arbitrarily defined and set to zero, to ensure that the recursion is well-defined.

# IV. PERFORMANCE ANALYSIS

This section evaluates the performance of the proposed OFFC method using a simplified SFR model for a system with 7500 MW of load. Simulations are carried out in MATLAB, and optimization is performed using GAMS. The test system represented by this second order SFR model is used to illustrate the general behavior of the proposed approach. The SFR model parameters are listed in Table I.

## A. Sensitivity Analysis

First, flattened system frequency response and required power injections are shown for different values of  $\beta$  in the system. As can be seen, for  $\beta > 1$ , the steady-state frequency is different from that of the original frequency response. This

TABLE I SFR MODEL PARAMETERS

Parameter	Value Parameter		Value	
R	0.05	$K_m$	0.95	
$T_{\rm r}$	8 s	D	1	
$F_H$	0.3	Н	4 s	

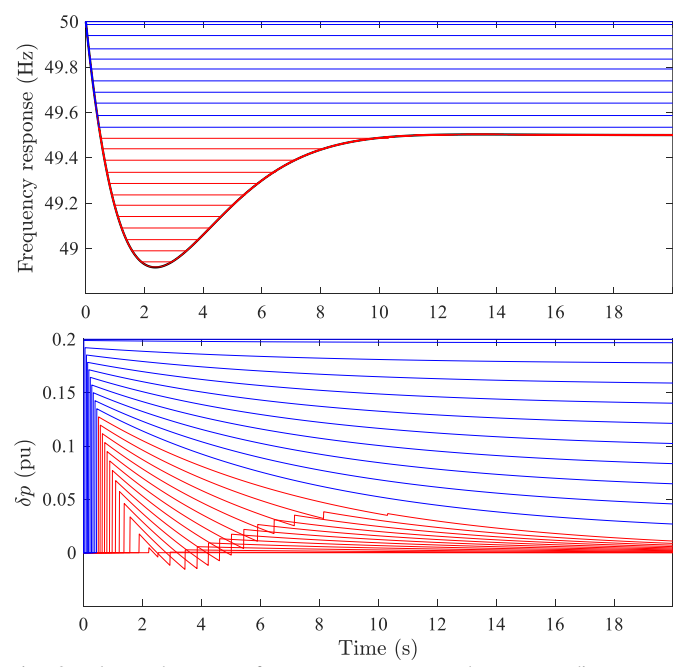


Fig. 3. Flattened system frequency response and corresponding power injections for different values of  $\beta$ .

explains the presence of non-decaying components in the injection profile. This in agreement with (8) where the second term is omitted. Now, a general sensitivity study is conducted to assess the impact of a range of factors on OFFC power profiles. Variations include changes in system inertia, load damping, and governor response speed. Results shown in Figs 3-5 confirm that the proposed method can provide effective nadir improvement across all tested scenarios with some short-lived power injections.

The capability of power injections to maximize frequency nadir is investigated under different pre-disturbance system conditions. It is observed that inertia plays a key role in the time of injection, but the energy needed for completely removing the transient deviation remains almost the same. The impact of load damping factor is very insignificant. This is contrary to the noticeable impact of the recovery time constant of the turbine governor  $(T_r)$  on system frequency response and injections needed to remove the frequency dynamic deviations.

# B. Optimization Results

In this subsection, the optimization framework is evaluated following the loss of 0.1 pu of generation capacity (750 MW) at t=1 sec. This leads to a frequency nadir of 49.45 Hz. A total of 80 generation resources are available, distributed across four types of technology as shown in Table II. The ramp-up and

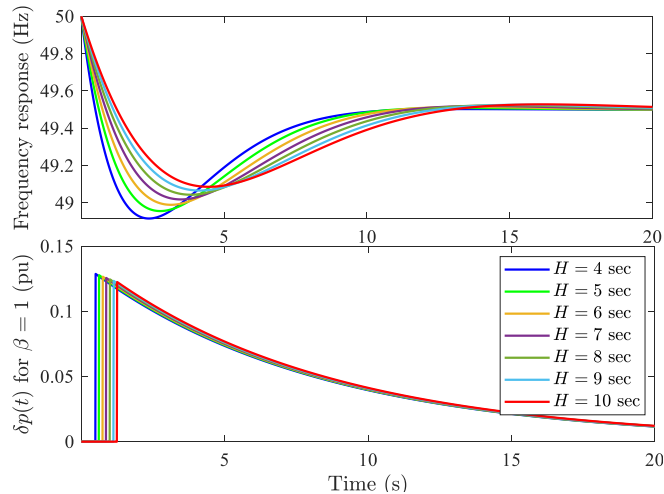


Fig. 4. The impact of system inertia on system frequency response and the power injections corresponding to  $\beta$ =1.

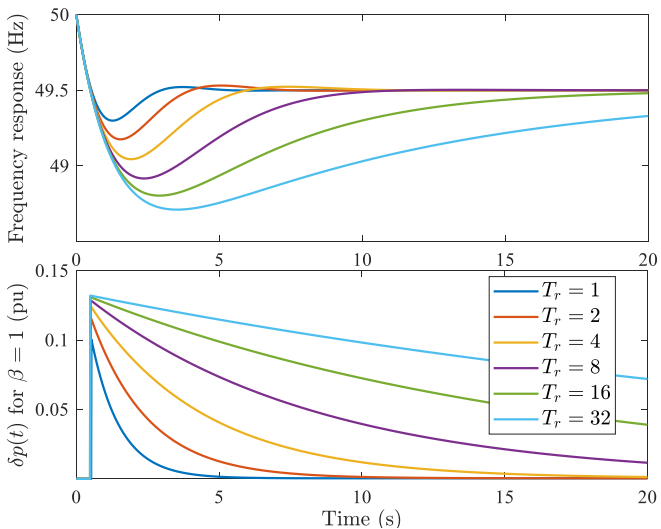


Fig. 5. The impact of turbine governor time constant on system frequency response and the power injections corresponding to  $\beta$ =1.

ramp-down rates are assumed equal for each type, and the delay time  $(T_{delay})$  accounts for detection and activation latency. The aggregate maximum power injection capability of the fleet is 1000 MW, with total energy of approximately 185 MWh.

Let us focus on a window of 20 seconds following the disturbance. If we are to halve the transient frequency deviation and maintain the frequency above 49.5 Hz during this period, a sustained injection of 450 MW for 20 seconds from the disturbance onset would be necessary, based on the traditional step-response concept. This would require an energy expenditure of 2.5 MWh. To the same end, however, the optimal frequency containment detailed in this paper suggests allocating short-term injections from diverse fast-acting resources to flatten the frequency response (with  $\beta = 1$ ).

The optimization problem is solved in GAMS using a simplified triangular target profile for the injection power  $\delta p_i^{trgt}$ , derived based upon the analytical formulations presented earlier. The triangle has a peak of 450 MW and starts

TABLE II
FAST-ACTING GENERATION RESOURCES

Technology	Pgmax (MW)	$R_k^{up,max}$ (MW/s)	T <sub>delay</sub> (s)	E <sub>g</sub> <sup>max</sup> (MWh)	No. of Units
BESS	10	20	0.5	2.5	50
PV-BESS	20	10	0.5	4	15
Flywheel	5	5	1	0.02	10
Wind	30	15	2	0.07	5

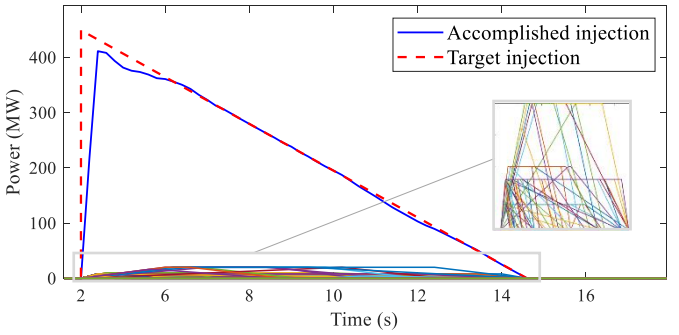


Fig. 6. Target and accomplished power injection profiles.

at t = 2 sec and lasts for almost 12 seconds. The resulting dispatch  $\delta p_i^{inj}$  is shown in Fig. 6 alongside the target profile, with magnified injection profiles of individual resources also illustrated. While some deviation exists between the target and the achievable injection, both yield significant improvements in system frequency stability. Specifically, the maximum frequency deviation is reduced from around 0.6 Hz (no control) to around 0.3 Hz (triangular injection). This improvement is achieved using only short-lived injections, with most resources ramping to full power in under two seconds and sustaining for durations proportional to their energy ratings. While all BESS and PV-BESS resources are used, only three of flywheels and none the wind resources are instructed to inject power for frequency containment. These results demonstrate that the proposed method can effectively coordinate diverse fast-acting resources to deliver rapid, targeted support following large disturbances, even with practical constraints such as ramp limits and activation delays.

## **CONCLUSIONS**

This work develops an integrated analytical-optimization framework for delivering optimal fast frequency containment following loss-of-generation events. This paper derives the precise power injection required to flatten the system's frequency response, ensuring maximum nadir improvement for a given injected energy. This theoretical optimum is directly linked to a real-time deployable target profile, enabling its practical realization. The proposed resource deployment formulation introduces a novel linear trapezoidal representation, allowing for accurate modeling of ramping constraints, activation delays, and energy limits without sacrificing computational tractability. By explicitly accommodating heterogeneous resource characteristics, the framework ensures that the aggregate system response closely follows the optimal injection profile. The results provide a scalable and deterministic approach that can be embedded in control center operations,

offering a pathway to enhanced stability in power systems with high penetration of renewables.

#### **APPENDIX**

To derive a closed-form solution for  $\pi_{\tau}(t)$ , we start by defining  $n_{\tau}(t)$  as below

$$n_{\tau}(t) = \Delta f(t+\tau)u(t) =$$

$$[\Delta f_{ss} + K_{\tau}\sin(\omega_d t + \varphi_{\tau}) e^{-\zeta \omega_n t}]u(t)$$
(A-1)

where  $\varphi_{\tau} = \omega_d \tau + \varphi$ ,  $K_{\tau} = K e^{-\zeta \omega_n \tau}$  and u(t) is the unit step function. The Laplace transform of  $n_{\tau}(t)$  is

$$N_{\tau}(s) = \frac{\Delta f_{ss}}{s} + K_{\tau} \left[ \frac{\sin \varphi_{\tau} s + \omega_n \sin(\varphi_{\tau} + \theta)}{(s + \zeta \omega_n)^2 + \omega_d^2} \right]$$
(A-2)

As described earlier,  $m_{\tau}(t)$  represents a time-shifted and downward-translated version of  $n_{\tau}(t)$ , given by

$$m_{\tau}(t) = \left[ \overbrace{n_{\tau}(t - \tau)}^{\Delta f(t)} - f_{\tau} \right] u(t - \tau)$$
 (A-3)

where  $\Delta f_{\tau} = \Delta f(\tau)$ . The Laplace transform of  $m_{\tau}(t)$  is

$$M_{\tau}(s) = N_{\tau}(s)e^{-s\tau} - \frac{\Delta f_{\tau}}{s}e^{-s\tau}$$
 (A-4)

Here, the term  $e^{-s\tau}$  corresponds to a rightward time shift by  $\tau$  in the time domain.

The signal  $\pi_{\tau}(t)$  represents the power injection input to the SFR model that produces the frequency deviation  $m_{\tau}(t)$  as output. Given the output, the corresponding input can be determined by applying the reciprocal of the SFR transfer function as below

$$\pi_{\tau}(t) = \mathcal{L}^{-1}\{M_{\tau}G_{SFR}^{-1}\}(t)$$
 (A-5)

where  $\mathcal{L}^{-1}\{.\}(t)$  denote the inverse Laplace transform and  $G_{SFR}^{-1}(s)$  represents the reciprocal of the SFR model. Substituting and rearranging, we have

$$\Pi_{\tau}(s) = M_{\tau}G_{SFR}^{-1} = \frac{\Delta f_{ss} - \Delta f_{\tau}}{s} \left[ \frac{(s + \zeta \omega_n)^2 + \omega_d^2}{\gamma s (T_R s + 1)} \right] e^{-s\tau}$$

$$+ K_{\tau} \left[ \frac{\sin \varphi_{\tau} s + \omega_n \sin(\varphi_{\tau} + \theta)}{\gamma (T_R s + 1)} \right] e^{-s\tau}$$
(A-6)

After bringing  $\Pi_{\tau}(s)$  to a common denominator, the coefficient of  $s^2$  in the numerator becomes zero. This is because as per (A-1), it can be seen that

$$n_{\tau}(0) = \Delta f_{\tau} = \Delta f_{SS} + K_{\tau} \sin \varphi_{\tau} \tag{A-7}$$

This implies that  $\Pi_{\tau}(s)$  has a first-order numerator and a second-order denominator. To apply partial fraction decomposition, the exponential term  $e^{-s\tau}$  (which corresponds to a time delay) is temporarily set aside. This intermediate step

facilitates the direct application of the initial and final value theorems to determine the coefficients. Therefore,  $\Pi_{\tau}(s)e^{s\tau}$  can be expressed as below

$$\Pi_{\tau}(s)e^{s\tau} = \frac{A^{\tau}}{s} + \frac{B^{\tau}}{s + \frac{1}{T_{P}}}$$
 (A-8)

The coefficient  $A_{\tau}$  and  $B_{\tau}$  can now be obtained by evaluating the limits implied by the initial and final value theorems:

$$\begin{cases} \pi_{\tau}(\tau^{+}) = \lim_{s \to +\infty} s\Pi_{\tau}(s)e^{s\tau} = A_{\tau} + B_{\tau} \\ \pi_{\tau}(+\infty) = \lim_{s \to 0^{+}} s\Pi_{\tau}(s)e^{s\tau} = A_{\tau} \end{cases}$$
(A-9)

Evaluating these limits using (A-6), we obtain:

$$A_{\tau} = (\Delta f_{ss} - \Delta f_{\tau}) \gamma^{-1} \omega_n^2 \tag{A-10}$$

$$B_{\tau} = \frac{K_{\tau}\omega_n \sin(\varphi_{\tau} + \theta) + 2\zeta\omega_n(\Delta f_{ss} - \Delta f_{\tau})}{\gamma T_R} - A_{\tau} \quad (A-11)$$

Hence, the closed form solution for the input signal  $\pi_{\tau}(t)$  is

$$\pi_{\tau}(t) = A_{\tau} u(t - \tau) + B_{\tau} e^{-\frac{(t - \tau)}{T_R}} u(t - \tau)$$
 (A-12)

#### REFERENCES

- [1] J. S. Cortés, M. R. Jegarluei, and S. Azizi, "Targeted fast frequency response by decomposing frequency into transient and steady-state deviations," in *Proc. IEEE Int. Conf. Energy Technol. Future Grids* (ETFG), Wollongong, Australia, 2023, pp. 1–6.
- [2] EU H2020 MIGRATE Project, D4.2 Limitations of present AC protection schemes and SIPS technologies to properly operate in systems with high penetration of PE during faults in DC and AC systems, Deliverable 4.2, Tech. Rep., 2017.
- [3] NERC, "Fast frequency response concepts and bulk power system reliability needs," Mar. 2020. Accessed: Apr. 3, 2025. [Online]. Available:https://www.nerc.com/comm/PC/IRPTF\_Webinars\_DL/2020-04\_Webinar-FFR\_White\_Paper.pdf
- [4] M. Sun, G. Liu, M. Popov, V. Terzija, and S. Azizi, "Underfrequency load shedding using locally estimated RoCoF of the center of inertia," *IEEE Trans. Power Syst.*, vol. 36, no. 5, pp. 4212–4222, Sep. 2021.
- [5] EU H2020 MIGRATE Project, D4.3 Development and tests of new protection solutions when reaching 100% PE penetration, Deliverable 4.3, Tech. Rep., Dec. 2018.
- [6] G. Frigo, A. Derviskadic, Y. Zuo, and M. Paolone, "PMU-based RoCoF measurements: Uncertainty limits and metrological significance in power system applications," *IEEE Trans. Instrum. Meas.*, vol. 68, no. 10, pp. 3810–3822, Oct. 2019.
- [7] J. Schiffer, P. Aristidou, and R. Ortega, "Online estimation of power system inertia using dynamic regressor extension and mixing," *IEEE Trans. Power Systems*, vol. 34, no. 6, pp. 4993–5001, Nov. 2019.
- [8] GE Grid Solutions, "Enhanced frequency control capability (EFCC), optimization detailed design," NG-EFCC-SPEC-004, Tech. Rep., 2016.
- [9] P. M. Anderson, Power System Protection. New York, NY, USA: IEEE Press, 1999.
- [10] P. M. Anderson and M. Mirheydar, "A low-order system frequency response model," *IEEE Trans. Power Syst.*, vol. 5, no. 3, pp. 720–729, Aug. 1990.
- [11] S. H. Horowitz, A. G. Phadke, and C. F. Henville, Power System Relaying, West Sussex, UK: John Wiley & Sons, 2022.